

## Supplementary Materials for

### Ultrasensitive and ultrathin phototransistors and photonic synapses using perovskite quantum dots grown from graphene lattice

Basudev Pradhan, Sonali Das, Jinxin Li, Farzana Chowdhury, Jayesh Cherusseri, Deepak Pandey, Durjoy Dev, Adithi Krishnaprasad, Elizabeth Barrios, Andrew Towers, Andre Gesquiere, Laurene Tetard, Tania Roy\*, Jayan Thomas\*

\*Corresponding author. Email: jayan.thomas@ucf.edu (J.T.); tania.roy@ucf.edu (T.R.)

Published 12 February 2020, *Sci. Adv.* **6**, eaay5225 (2020)  
DOI: 10.1126/sciadv.aay5225

#### This PDF file includes:

Supplementary Text

Section S1. Mobility calculation

Section S2. Pattern recognition

Fig. S1. PQD growth mechanism on single-layer graphene.

Fig. S2. XPS core level spectra of pristine PQDs.

Fig. S3. XPS core level spectra of G-PQDs.

Fig. S4. PQDs grown from graphene surface.

Fig. S5. Graphene FET.

Fig. S6. Shift of Dirac point due to PQDs grown on graphene.

Fig. S7. Transient photocurrent response.

Fig. S8. Calculation of PPF from the transient characteristic of the device for two consecutive light pulses.

Fig. S9. STP to LTP.

Fig. S10. Strategy to get testing dataset, which should be different from the images in the training dataset.

Fig. S11. Synaptic weights of each output neurons from the training of MNIST dataset.

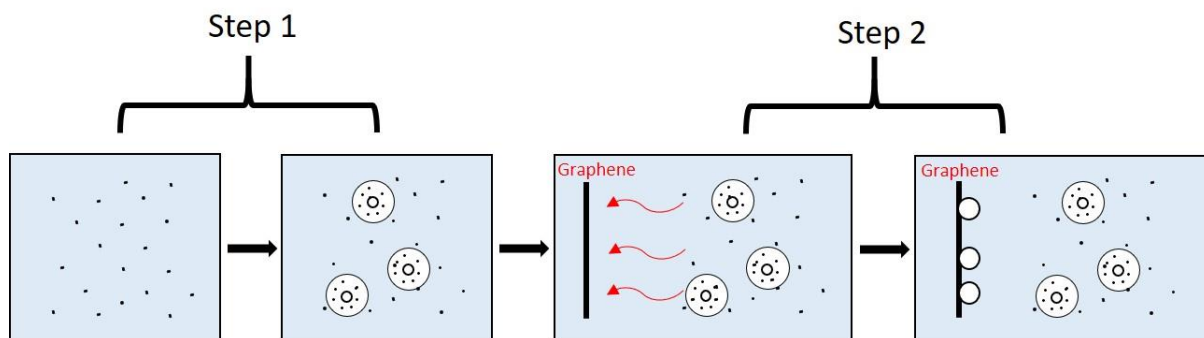
Fig. S12. Fitted conductance change with pulse number of synapse.

Table S1. Comparison of our work with previously reported works in the literature in terms of energy consumption.

Table S2. Fitting parameters for potentiation and depression.

References (43–48)

## Supplementary Text



**Fig. S1. PQD growth mechanism on single-layer graphene.**

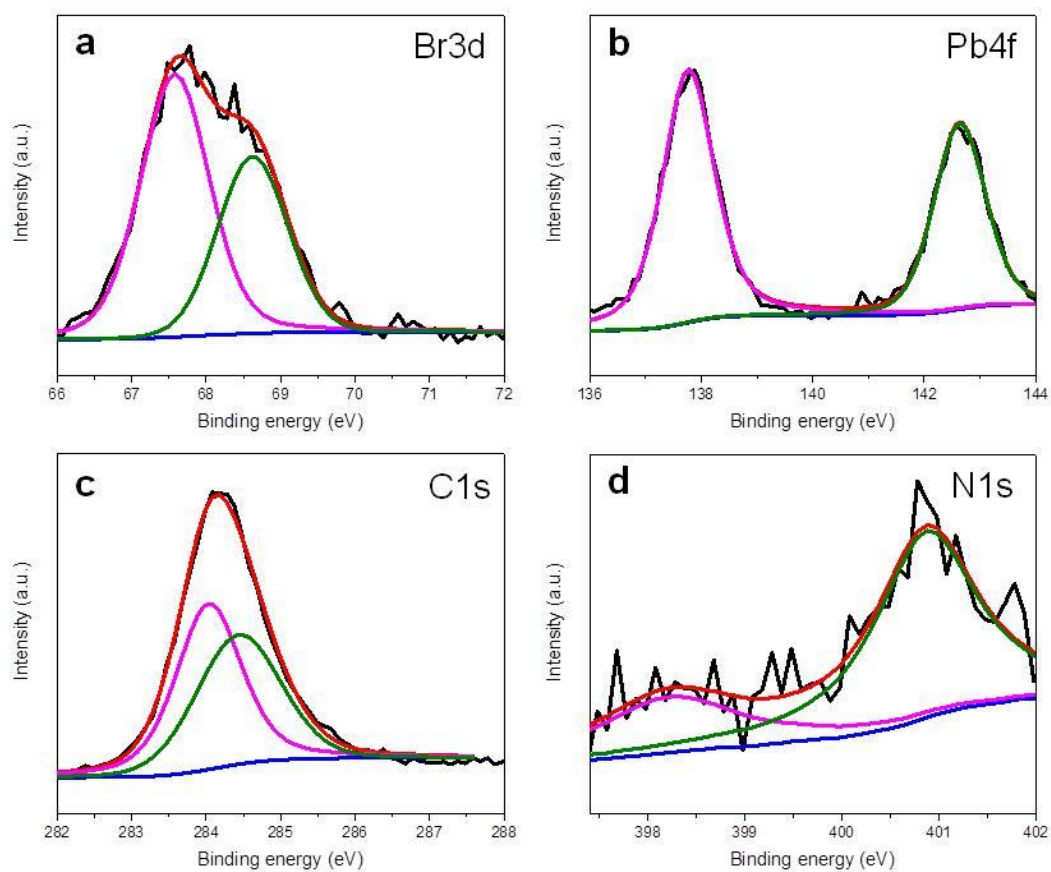


**Fig. S2. XPS core level spectra of pristine PQDs: Br3d (a), Pb4f (b), C1s (c), and N1s (d) spectra of pristine PQDs.**

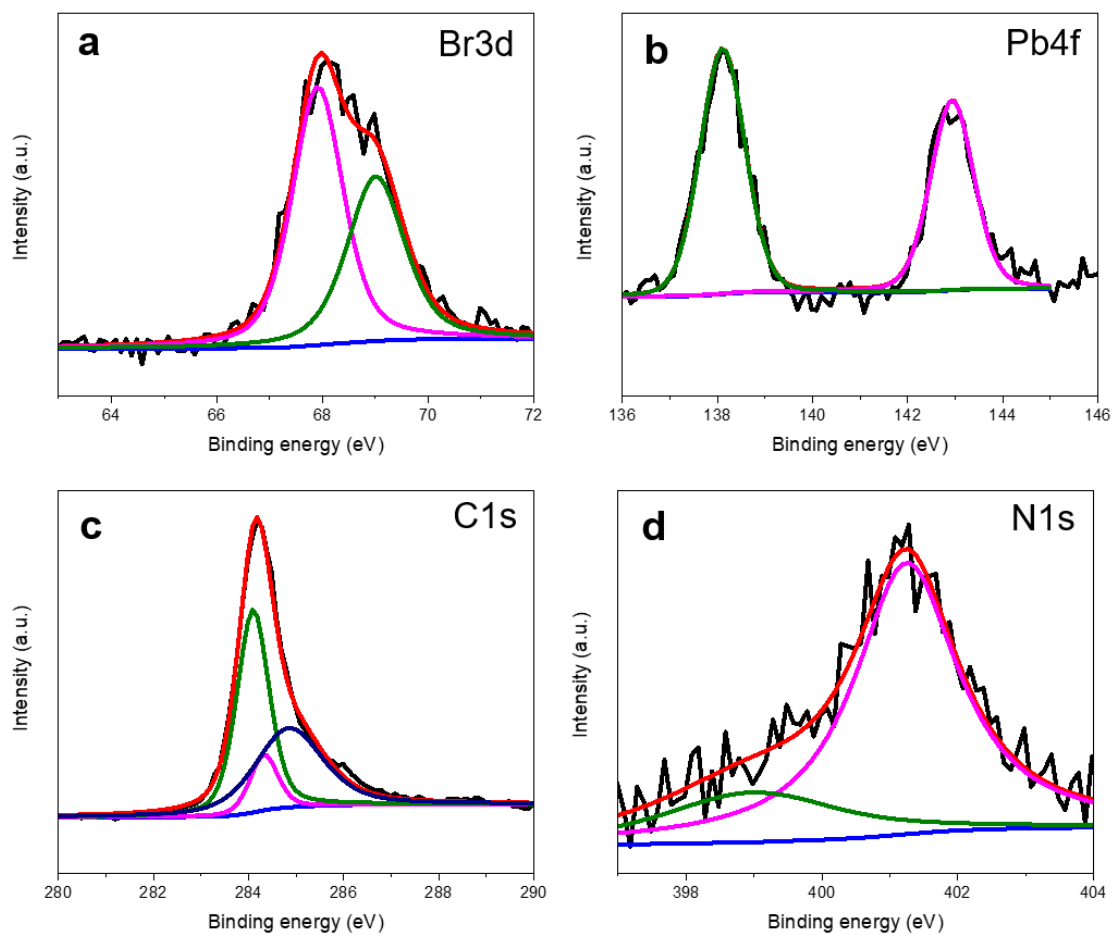


**Fig. S3. XPS core level spectra of G-PQDs: Br3d (a), Pb4f (b), C1s (c), and N1s (d) spectra of G-PQDs.**

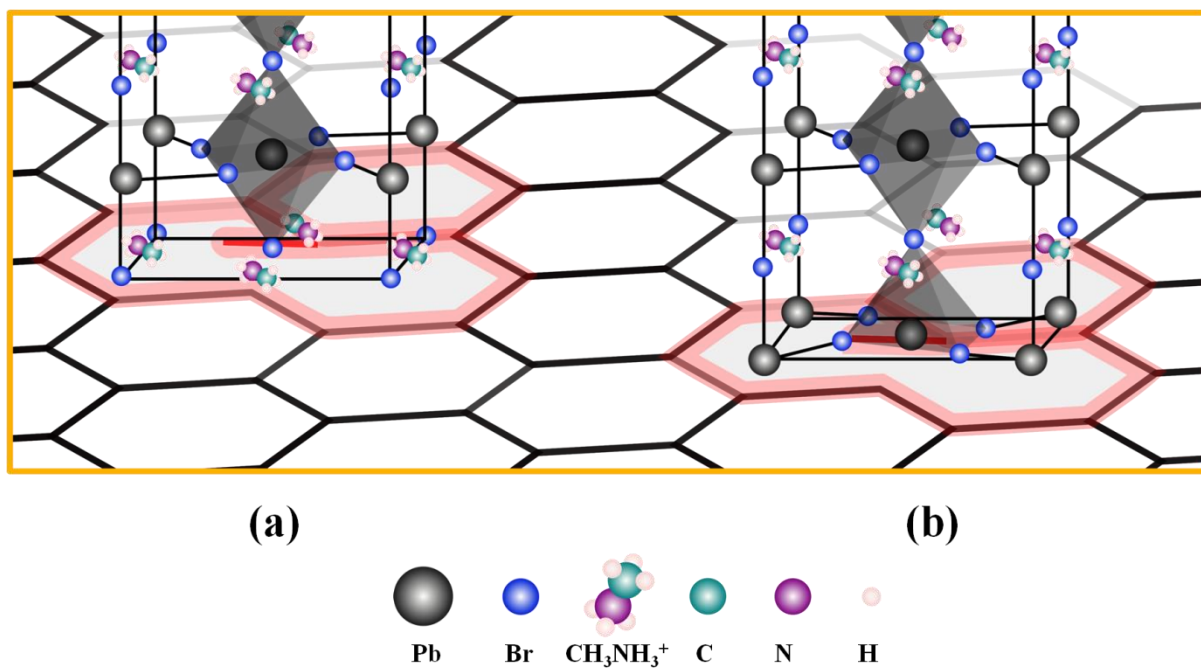


**Fig. S4. PQDs grown from graphene surface.** (a) Methylammonium Bromide termination (MABr-T), (b) Lead Bromide termination (PbBr-T). (Color codes of spheres: dark gray: Lead; Dark Blue: Bromine; Sky Blue: Carbon; purple: Nitrogen; pink: Hydrogen), Photo Credit: Deepak Pandey, UCF and David Fox, UCF.

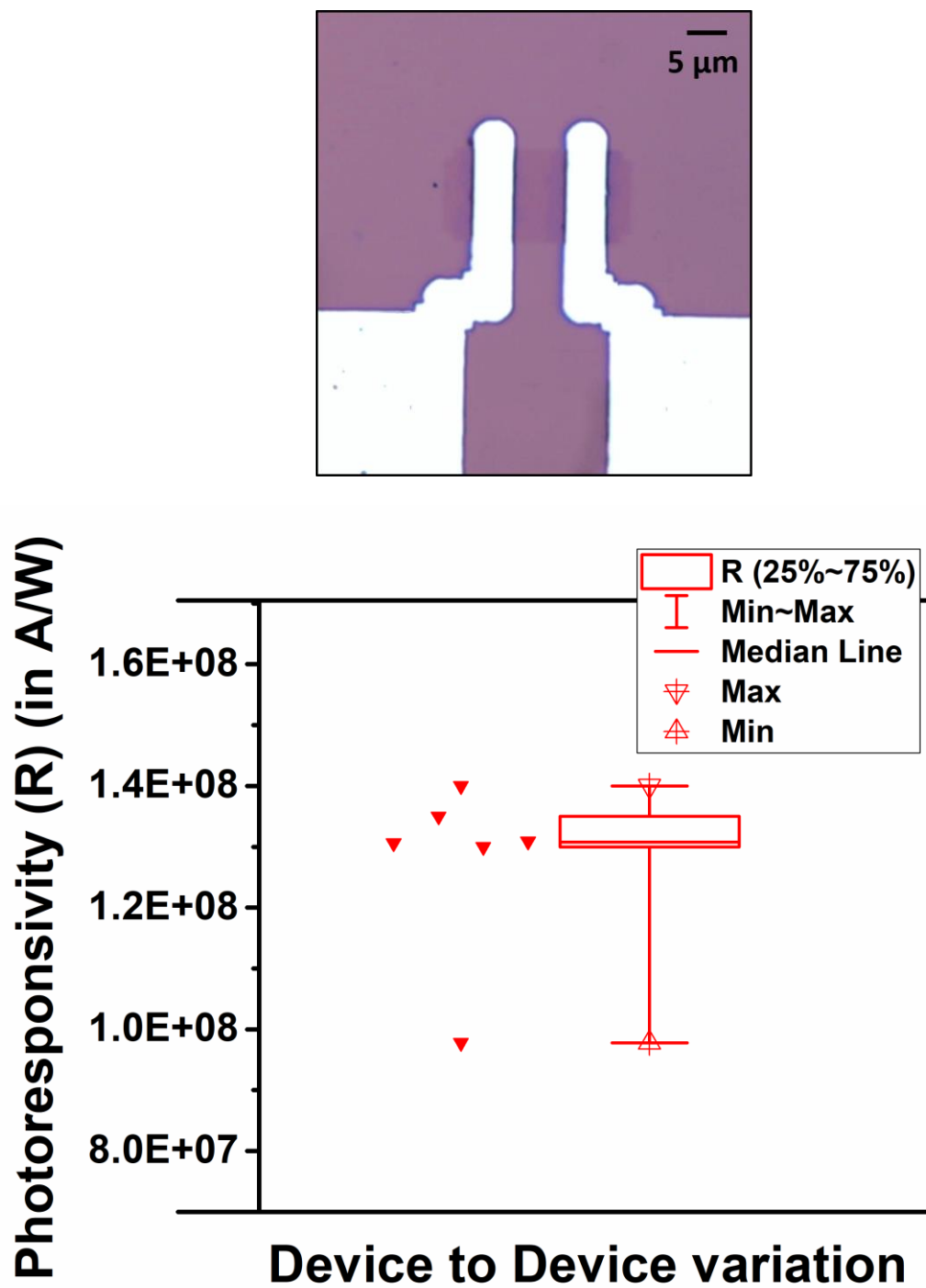


**Fig. S5. Graphene FET.** (a) Optical images of the pristine graphene device on SiO<sub>2</sub>/Si substrate before growth of the PQDs. (b) Reproducibility: Device to device variation of G-PQDs superstructure with respect to the measured photoresponsivity (R) in A/W.

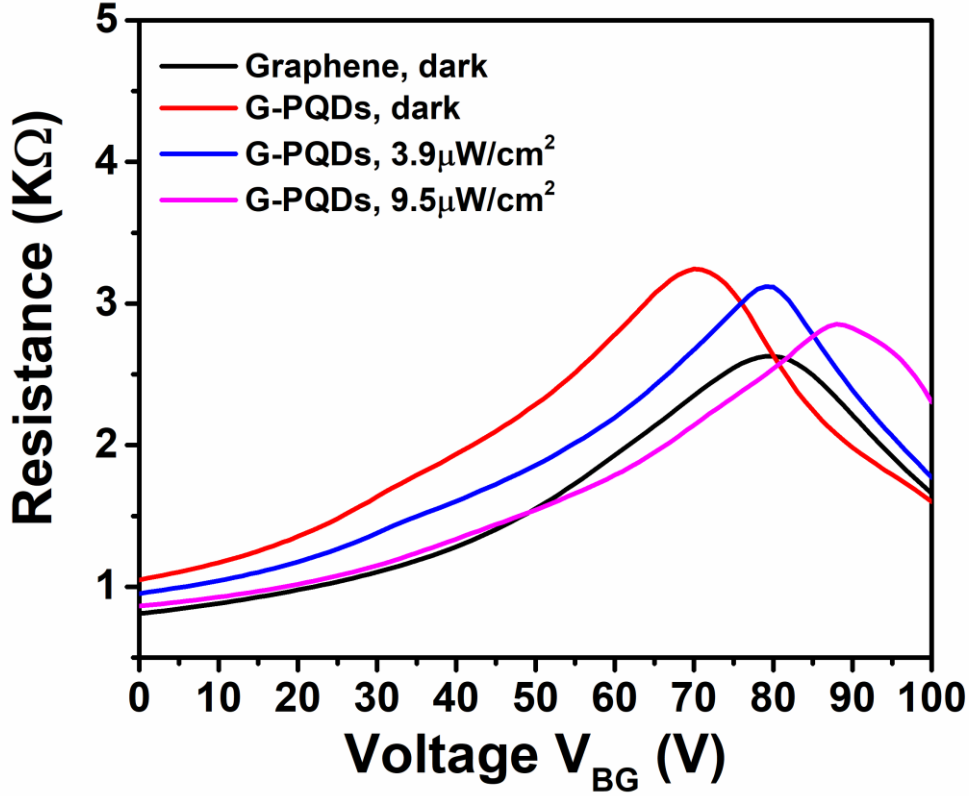


**Fig. S6. Shift of Dirac point due to PQDs grown on graphene.** Resistance as function of back gate voltage for G-PQDs superstructure before (black) and after PQD growth on graphene in dark conditions (red), at illumination (437 nm) of  $3.9 \mu\text{W}/\text{cm}^2$  (blue) and at illumination (437 nm) of  $9.5 \mu\text{W}/\text{cm}^2$  (pink).

### Section S1. Mobility calculation

To calculate the mobility of the graphene channel (with and without PQD), total resistance of the device is plotted as a function of the back gate voltage ( $V_{BG}$ ) and the dirac point ( $V_{dirac}$ ) has been noted down. Using a back gate capacitance ( $C_{BG}$ ) corresponding to the  $\text{SiO}_2$  insulating layer and neglecting the quantum capacitance of graphene (since it is much larger than the insulator capacitance), the carrier concentration;  $n(V_{BG})$  is obtained by the following equation.

$$n(V_{BG}) = \frac{C_{BG}}{e} |V_{BG} - V_{dirac}| \text{ where, } e \text{ is the electronic charge.}$$

In a transistor, where carriers transport can be described by drift-diffusive model<sup>43</sup>, the total resistance is described by

$$R_{tot} = R_c + \frac{L}{W} \frac{1}{e\mu\sqrt{n_0^2 + n(V_{BG})^2}}$$

where  $R_c$  considers the contact resistance between source/drain,  $L$  and  $W$  specify the length and width of the channel respectively and  $n_0$  is the residual carrier concentration and  $\mu$  is the mobility of the channel. By fitting this model to the measured data (Fig. S6), we can extract the mobility along with other parameters like  $n_0$  and  $R_c$ .

## Photonic Synapses

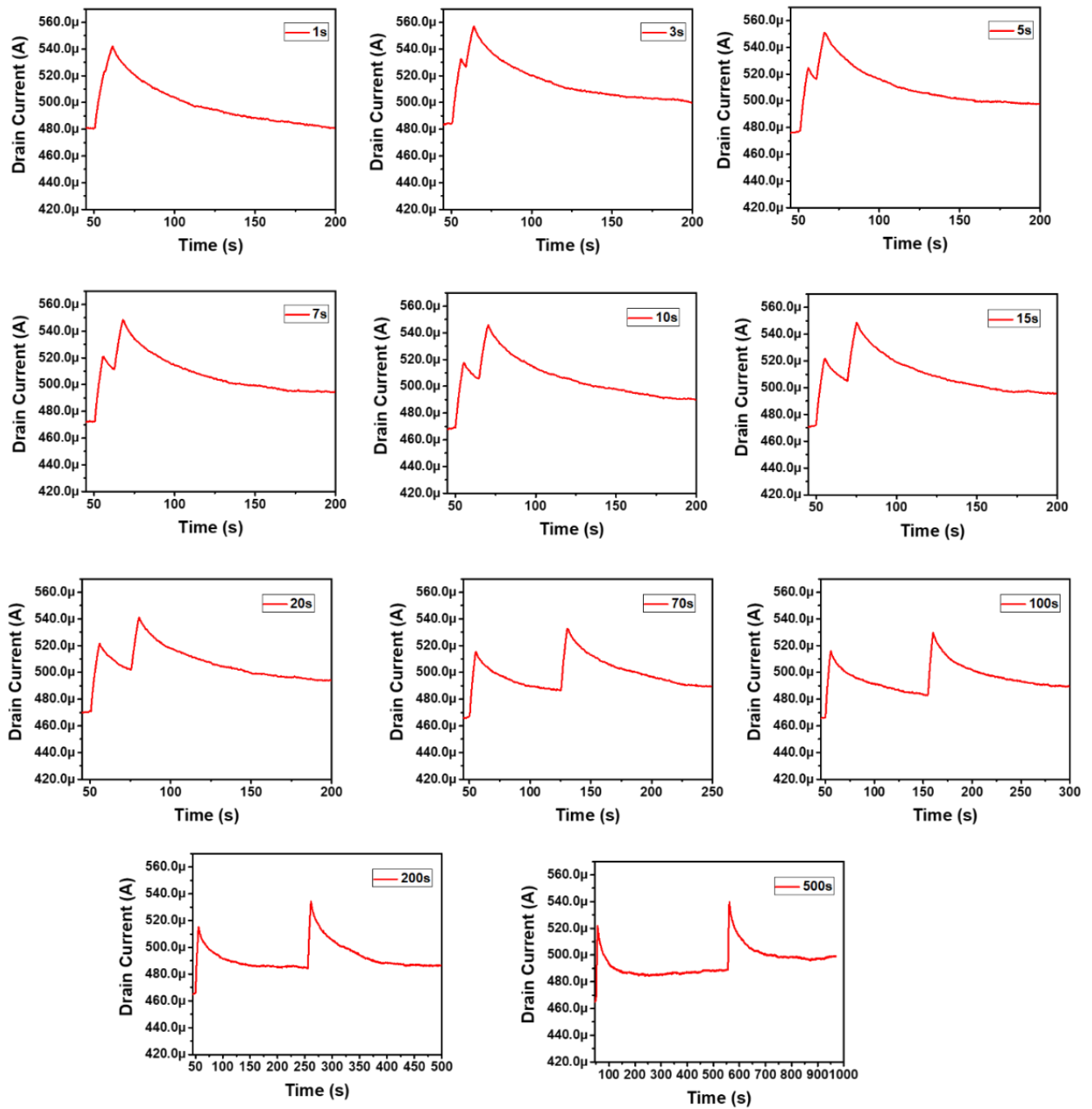


**Fig. S7. Transient photocurrent response.** Transient characteristic of the device ( $V_D = 0.5$  V,  $V_G = 10$  V) showing the change in drain current due to a varying the off time (or delay) between two consecutive light pulses having pulse width of 5 s. Light intensity and wavelength remain constant at  $1.1 \mu\text{W}/\text{cm}^2$  and 440 nm respectively.

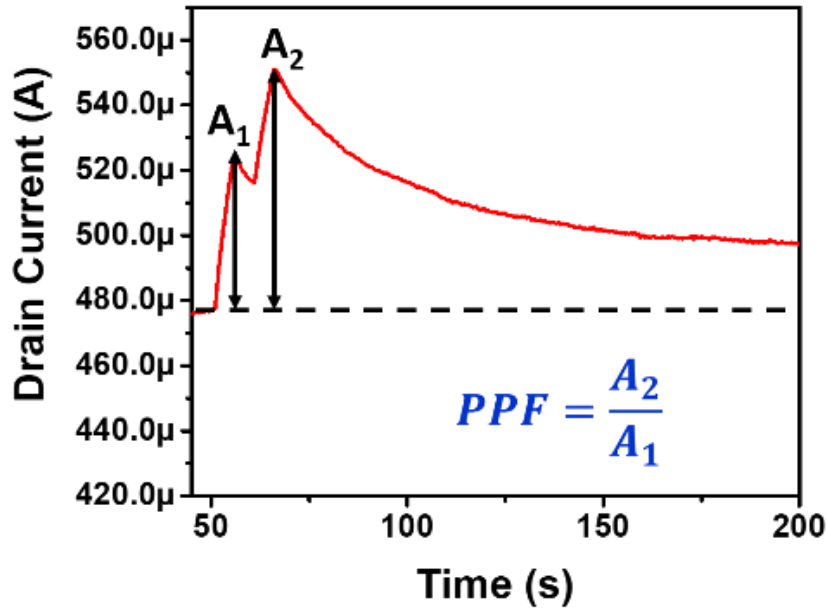


Fig. S8. Calculation of PPF from the transient characteristic of the device for two consecutive light pulses.

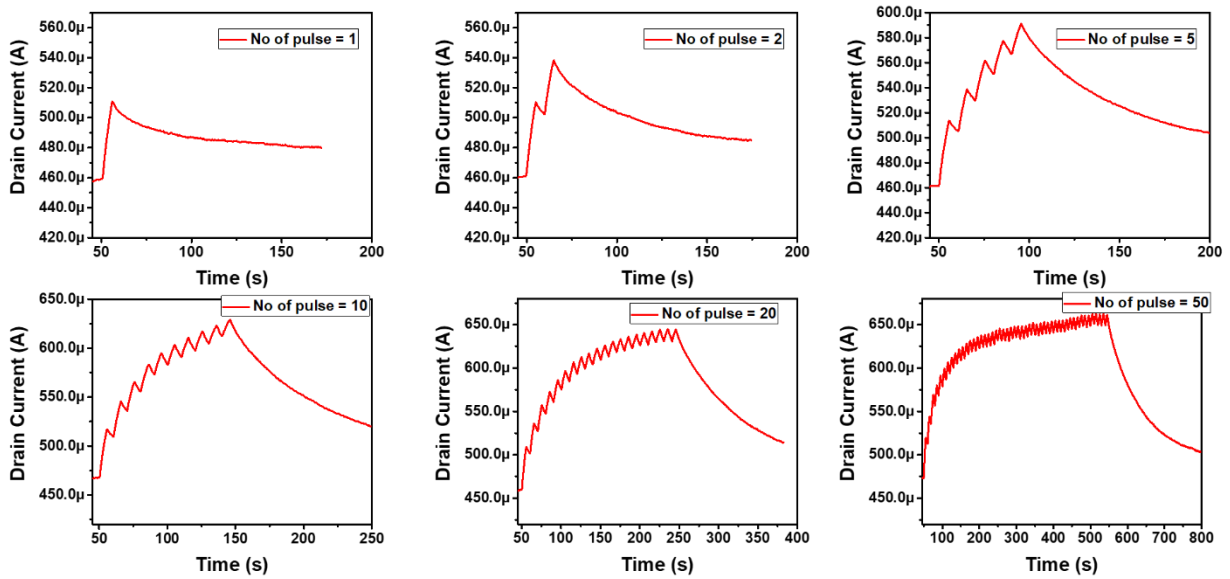


Fig. S9. STP to LTP. Transient characteristic of the device ( $V_D = 0.5$  V,  $V_G = 10$  V) showing the change in drain current due to varying number of light pulses (1, 2, 5, 10, 20, 50) having on/off time of 5 s/5 s. Light intensity and wavelength remain constant at  $1.1 \mu\text{W}/\text{cm}^2$  and 440 nm respectively. The ratio of the final current to the initial current tends to increase as number of pulses increases. This clearly depicts the transition of the device from short term plasticity to long term plasticity.



**Table S1. Comparison of our work with previously reported works in the literature in terms of energy consumption.**

<b>Active layer</b>	<b>Spike Wavelength (nm)</b>	<b>Energy consumption (nJ)</b>	<b>Ref</b>
2D perovskite/ Graphene	520	0.592	44
Carbon nanotube/ Graphene	405 and 532	250	45
C8-BTBT	360	2160	46
Indium gallium zinc oxide (IGZO)– aluminum oxide (Al <sub>2</sub> O <sub>3</sub> ) thin film structure	365	2.4	47
IGZO thin film	380	3.0	48
CsPbBr <sub>3</sub> /PMMA/pentacene	365	76.5	36
<b>Perovskite quantum dot/ Graphene</b>	<b>430</b>	<b>0.0367</b>	<b>This work</b>

## Section S2. Pattern recognition

For pattern recognition, we conducted both facial recognition and number recognition. For facial recognition, we used portraits from 4 persons. In order to have testing dataset which has different images from the training set, we vary the light intensity and the face angle, which is shown in Fig. S10. The input neuron size is 7000, which is equal to the total pixels of one portrait ( $100 \times 70$ ). The output neuron size is 10 in order to have good accuracy. For MNIST dataset, the input neuron size is 784 ( $28 \times 28$ ) and the output neuron size is 64. The results of MNIST dataset recognition are shown in Fig. S11, which show the synaptic weights of each output neurons and the accuracy is around 44.1% after 10 epochs.



**Fig. S10. Strategy to get testing dataset, which should be different from the images in the training dataset.** Photo credit: Sreekanth Varma & Basudev Pradhan.

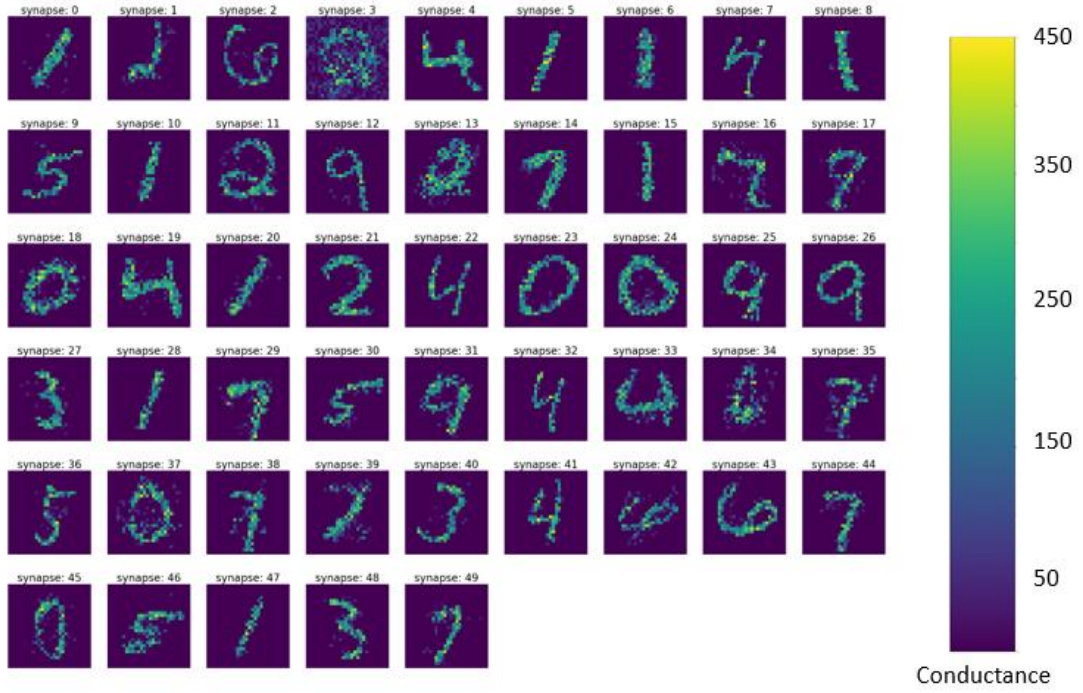


**Fig. S11. Synaptic weights of each output neurons from the training of MNIST dataset.**

For simulation, we followed the protocols described in<sup>41</sup>. They were focused on electrical synapses while for our photonic synapses, both optical and electrical signals are used to change the conductance of the device. The add-on sensors will sense the external environmental signals and then transform them to presynaptic spikes. The postsynaptic current is integrated by output neurons. Once the summed postsynaptic current is beyond the threshold, the output neuron spikes and this signal goes back to the synapse to adjust its property with the input presynaptic spike. Compared to electrical synapses, the chip realization of our photonic synapses might need optical/electrical switch as well as both optical and electrical spike realizations. An increase or decrease of the device conductance is fitted by

$$\Delta G = a_p + b_p e^{-c_p \frac{G - G_{min}}{G_{max} - G_{min}}}$$

$$\Delta G = a_d + b_d e^{-c_d \frac{G_{max} - G}{G_{max} - G_{min}}}$$

However, in real biological system, the weight change of the synapse is also related to the time interval between the pre and post synaptic spikes. In our case, we considered the simplified STDP learning rule without considering the time interval effect, which makes the neuron circuits much easier to develop.

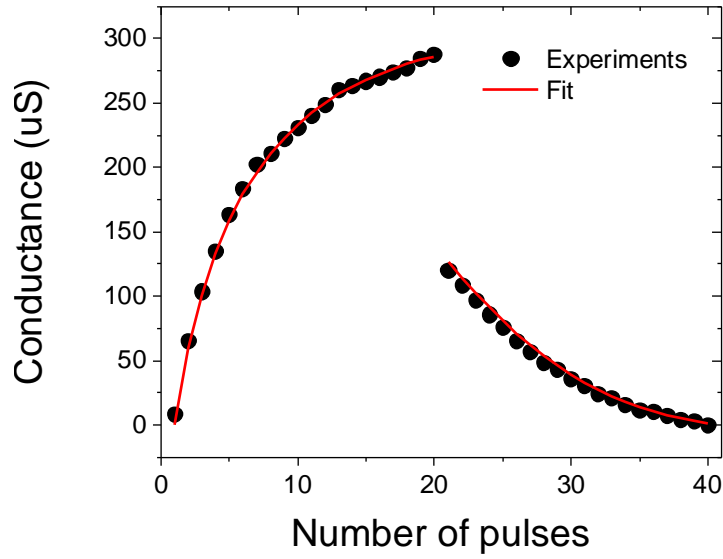


**Fig. S12. Fitted conductance change with pulse number of synapse.**

Neurons are leaky integrate-and-fire types, which integrate postsynaptic currents and spike once the currents reach the threshold. The characteristic can be modeled by a simple equation

$$\frac{dV}{dt} = \frac{I_{post} - GV}{\tau}$$

where  $\tau$  is a time constant,  $V$  is the state variable (voltage) of the neuron and  $I_{post}$  is the summed post synaptic current which goes into the output neuron. In addition, to mimic the homeostasis inside of biological system, the following equation is included in the simulation for output neurons

$$\frac{dV_{th}}{dt} = \gamma(A - T)$$

where  $A$  is the mean firing rate of a neuron,  $T$  is the target firing rate and  $\gamma$  is a constant. The role of homeostasis is to adjust the thresholds of neurons. The meaning of the homeostasis is to adjust the thresholds of neurons. If the mean fire rate of the neuron is above the target, the threshold of this neuron will increase. This is to make sure all the output neurons are used and make each one specialized for the stimuli.

We performed unsupervised machine learning by simulation, of which the label work is done after training. After training/learning, we labeled each output neuron with its corresponding figure. Then when testing, we input different dataset from the training dataset and check the accuracy of the output with the labeling.

**Table S2. Fitting parameters for potentiation and depression.**

	<b>a</b>	<b>b</b>	<b>c</b>	<b>Gmax (uS)</b>	<b>Gmin (uS)</b>
Potentiation	-28.98866	87.6852	1.03342	288	0.01
Depression	17.05051	-1.04423	-2.70541	288	0.01